Alignment dependence of photoelectron momentum distributions of atomic and molecular targets probed by few-cycle circularly polarized laser pulses

M. Abu-samha
College of Sciences and Humanities, Fahad bin Sultan University, P.O. Box 15700, Tabuk 71454, Saudi Arabia

Lars Bojer Madsen
Department of Physics and Astronomy, Aarhus University, 8000 Aarhus C, Denmark
(Received 14 June 2016; published 22 August 2016)

We present theoretical photoelectron momentum distributions (PMDs) for ionization from Ar($3p$) and $H_2^+(\sigma_g)$ orbitals by few-cycle, high-intensity, near-infrared laser fields circularly polarized in the xy plane. The three-dimensional time-dependent Schrödinger equation is solved numerically within the single-active-electron approximation for Ar and within the fixed nuclei approximation for H_2^+. The PMDs are investigated for alignment of the probed target orbitals relative to the polarization plane of the laser field. In the atomic case, the PMDs in the polarization plane for aligned $3p$ Ar orbitals are, up to an overall scaling factor, insensitive to alignment of the probed orbital, while the lateral PMDs show a signature of the orbital node when that node is sufficiently close to the polarization plane. For the molecular case of $H_2^+(\sigma_g)$, our results show a significant impact of alignment on the PMDs due to the anisotropic molecular potential and the alignment-dependent coupling between the ground state and excited states.

DOI: 10.1103/PhysRevA.94.023414

I. INTRODUCTION

In strong-field photoionization experiments with near-infrared (NIR) light, the external field distorts the atomic potential, and electrons may be liberated. The most common experimental measurements are those of total ionization yield (TIY), above-threshold ionization (ATI) spectra, and photoelectron momentum distributions (PMDs). Strong-field ionization studies have, e.g., addressed the roles of the laser field and carrier-envelope phase effects [1–7], the electronic structure and symmetry of the probed orbital [8,9], and photoionization dynamics (tunneling ionization vs multiphoton ionization via low-lying Rydberg states [10,11]). Recently, strong-field experiments and theory target information on real-time observation of atomic-scale electron dynamics, including attosecond streaking [12], strong-field circular dichroism [13,14], and attosecond ionization dynamics as exemplified by attoclock experiments and theory [15–22].

Strong-field ionization of atoms [13,16,23,24] and molecules [25–32] by femtosecond, circularly and elliptically polarized lasers has become a subject of intense experimental and theoretical investigation. Measurements of the PMDs of atomic targets probed by a few-cycle close to circularly polarized laser [15,16,19] reveal an offset angle in the PMDs, relative to the predictions of the simple model (sometimes called "simple man's model") in which the atomic potential is omitted, and the final momentum of the electron is determined classically by the force of the external field. The offset angle depends both on the laser intensity and frequency; that is, the offset angle in PMDs decreases by going to higher laser intensity [19,33,34]. The offset angle has been associated with a possible tunneling time delay [15,16,35]. Physically, the offset angle and the rotation of the PMD compared to the expectation from the simple man's model are due to the interaction of the outgoing electron with the atomic or molecular potential [36], a point that will become particularly clear from the calculations of PMDs for aligned H_2^+ presented below.

In strong-field ionization of molecules, the nature of the probed targets has additional effects on the PMDs: scattering due to multicenter character [33,37], coupling of electronic and nuclear motions [38], and multielectron effects [39] have been investigated. Strong-field studies of H_2^+ [33,40–43] addressed the role of Coulomb potential, coupling of nuclear and electronic motion, and light-induced subcycle dynamics and how these factors impact ATI and PMDs. Also effects of a possible induced or static molecular dipole potential have been investigated [25,27–29,31,32]. In Ref. [33], the calculations for elliptical and circularly polarized light were performed in two dimensions, and the resulting PMDs reveal an offset angle which is a function of both intensity and wavelength. To the best of our knowledge, previously reported theoretical PMDs for H_2^+ in NIR circularly polarized light were obtained from solutions of the two-dimensional (2D) time-dependent Schrödinger equation (TDSE) with fixed nuclei and the molecule confined to the plane of polarization. For linearly polarized light three-dimensional (3D) TDSE studies of PMDs from aligned H_2^+ were previously reported [44–46].

In this paper we address the question about the sensitivity of the PMDs following strong-field ionization to the alignment of the target orbital relative to the plane of the circular laser polarization and the shape of the atomic or molecular potential. We do so by performing calculations in two different systems. First, we consider the 3D TDSE for Ar with an aligned $3p$ orbital as the initial state. In this case, the potential is spherically symmetric, and therefore this part of the study allows us to isolate the effect of alignment on the PMD and also on TIY and ATI. Second, we solve the 3D TDSE for aligned $H_2^+(\sigma_g)$ in the fixed-nuclei approximation. In this case the asymmetry of the molecular potential in the polarization plane depends on the alignment of the molecule with respect to that plane. Our investigations of the alignment

dependence of the ionization of the aligned Ar $3p$ orbital show that the PMDs in the plane of polarization and ATI spectra are insensitive to orbital alignment. Only the lateral PMD and the TIY change with the alignment. Turning to H_2^+, our investigations of PMDs indicate that the momentum distributions are strongly affected by the orbital alignment and are therefore very sensitive to the anisotropy of the molecular potential and the alignment-dependent excitation out of the ground state.

This paper is organized as follows. In Sec. II we provide a summary of the methodology we use to solve the TDSE. In Sec. III we discuss our results, first for Ar and then for H_2^+. Section IV summarizes and concludes. Atomic units are used throughout.

II. METHODOLOGY AND COMPUTATIONAL DETAILS

The time-dependent wave function is expanded in spherical harmonics $Y_{lm}(\Omega)$ for the angular degrees of freedom Ω

$$\Psi(\boldsymbol{r},t) = \sum_{l=0}^{l_{max}} \sum_{m=-l}^{l} \frac{f_{lm}(r,t)}{r} Y_{lm}(\Omega), \tag{1}$$

and the TDSE is solved in the velocity gauge with a grid representation for the reduced radial wave functions $f_{lm}(r,t)$ [47]. We obtain an improved scaling with the maximal orbital quantum number l_{max} retained in the sum in Eq. (1) by applying Wigner transformations between the body-fixed frame and the frame of the instantaneous electric field [47,48], a methodology that was recently successfully extended to fully six-dimensional calculations in helium [49–51].

The external circularly polarized laser pulse is described by $\vec{F}(t) = -\partial_t \vec{A}(t)$, where $\vec{A}(t)$ is the vector potential, given as

$$\vec{A}(t) = \frac{A_0}{\sqrt{2}} f(t) \begin{pmatrix} \cos(\omega t - \pi/2) \\ \sin(\omega t - \pi/2) \\ 0 \end{pmatrix}, \tag{2}$$

with A_0 being the amplitude, ω being the carrier angular frequency, and $f(t) = \sin^2(\omega t/2N)$ being the envelope for an N-cycle pulse. In the present work, $\omega = 0.057$ a.u., corresponding to a wavelength of 800 nm, $N = 3$ for Ar ($N = 2$ for H_2^+), and a time step of $\Delta t = 0.005$ a.u. is used in our split-step Crank-Nicolson propagator.

We carried out TDSE calculations for the Ar($3p_z$) and $H_2^+(\sigma_g)$ orbitals at alignment angles $\beta = 10^\circ, 20^\circ, \ldots, 90^\circ$ with respect to the xy-polarization plane of the laser field (Fig. 1).

For Ar, the calculations are performed at a peak laser intensity of 0.1 PW/cm^2. We use an equidistant radial grid with 4096 points that extends up to 400 a.u. The expansion in Eq. (1) is truncated at $l_{max} = 40$. The single-active-electron potential describing Ar is taken from Ref. [52]. PMDs are computed by projecting the wave packet at the end of the laser pulse on scattering states (see, e.g., Refs. [53,54] for discussions of ways to extract observables from wave packets). The scattering states are obtained from the radial Schrödinger equation using the same radial grid, size of angular basis set l_{max}, and atomic potential as in the TDSE calculations.

For H_2^+, we consider a frozen geometry with an internuclear distance of 5 a.u., a radial grid (4090 grid points) that extends to 600 a.u., and $l_{max} = 60$. The calculations are performed at peak laser intensity of 0.2 PW/cm^2. As we discuss and validate below, PMDs are obtained by projecting the asymptotic part of the wave packet on Coulomb scattering states [53] to avoid using exact scattering states.

III. RESULTS AND DISCUSSION

A. Strong-field ionization of Ar($3p_z$): Alignment angle and TIY, PMDs, and ATI

In atoms, the spherically symmetric potential supports aligned states, and therefore Ar($3p_z$) serves as a good case for isolating effects of orbital alignment in strong-field ionization [8,9]. In this section, we investigate the sensitivity of TIY, PMDs, ATI, and lateral momentum distributions to alignment. By definition, the $3p_z$ orbital is aligned along the body-fixed z axis. We refer to this axis as the body-fixed or the molecular-fixed z axis z^M (Fig. 1). At alignment angle $\beta = 0^\circ$, the molecular- and laboratory-frame axes coincide, and the laser field thus runs through the angular node of the $3p_z$ orbital. At $\beta = 90^\circ$, the molecular frame is rotated by 90° around y^L, and hence the initial body-fixed $3p_z$ orbital is aligned parallel to the x^L axis; that is, at $\beta = 90^\circ$ the $3p_z$ orbital has been rotated into the laboratory-fixed $3p_x$ orbital and has maximum overlap with the laser field. In the following, coordinates without a superscript will refer to the laboratory-fixed frame.

First, we present TIY for Ar($3p_z$) at different β angles in Fig. 2. As anticipated from a simple geometrical picture where the ionization yield reflects the electron density in the polarization plane, Ar($3p_z$) has the greatest TIY at $\beta = 90^\circ$, and the TIY decreases monotonously with decreasing β. Next, we discuss the PMDs for the $3p_z$ orbital at different alignment angles β. By interrogating the PMDs, one may be able to shed light on the effect of orbital alignment on the offset angle observed in PMDs. In Fig. 3, we present PMDs in the polarization plane for the Ar($3p_z$) orbital at

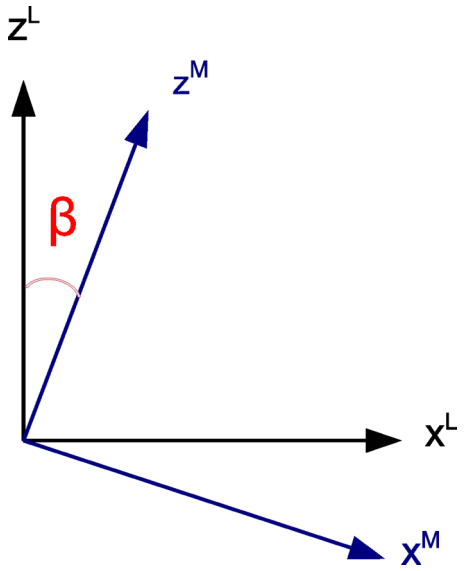

FIG. 1. Laboratory frame ($x^L z^L$) vs molecular frame ($x^M z^M$). At $\beta = 0^\circ$, the coordinate systems are aligned. At $\beta = 90^\circ$, $z^M = x^L$ and $x^M = -z^L$. The PMDs presented here are computed in the laboratory frame.

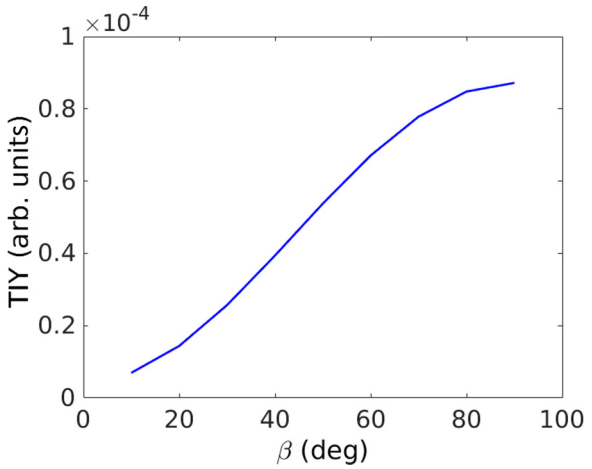

FIG. 2. Total ionization yield (TIY) from Ar($3p_z$) at different alignment angles β (see Fig. 1). The parameters of the circularly polarized laser are as follows: intensity of 0.1 PW/cm^2, pulse duration of three cycles, and wavelength of 800 nm.

different alignment angles β. The PMDs were renormalized to the same maximum differential probability. The obtained PMDs are typical for a p-type initial orbital probed by few-cycle elliptically polarized laser pulses (see, for example, Refs. [36,55,56] for a detailed interpretation of the PMDs). Figure 3 shows that the renormalized PMDs obtained at different β values are very similar, and we conclude that the PMDs in the polarization plane are insensitive to orbital alignment relative to the polarization plane of the laser field in the case of a spherically symmetric potential. Effects of changing the carrier-envelope phase were discussed in Ref. [4].

To provide a quantitative analysis of the PMDs of Ar($3p_z$) and its β dependence, we present ATI spectra in Fig. 4(a). The

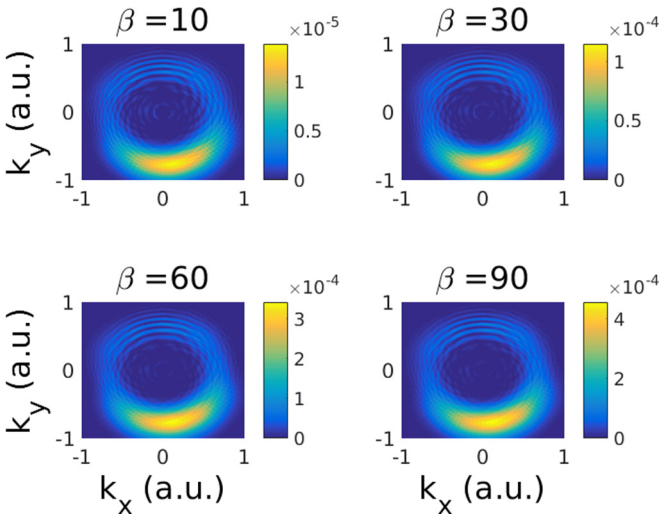

FIG. 3. PMDs for Ar($3p_z$) at various alignment angles β (in in degrees) of the orbital relative to the polarization plane of the laser field. The parameters of the circularly polarized laser are as follows: intensity of 0.1 PW/cm^2, pulse duration of three cycles, and wavelength of 800 nm.

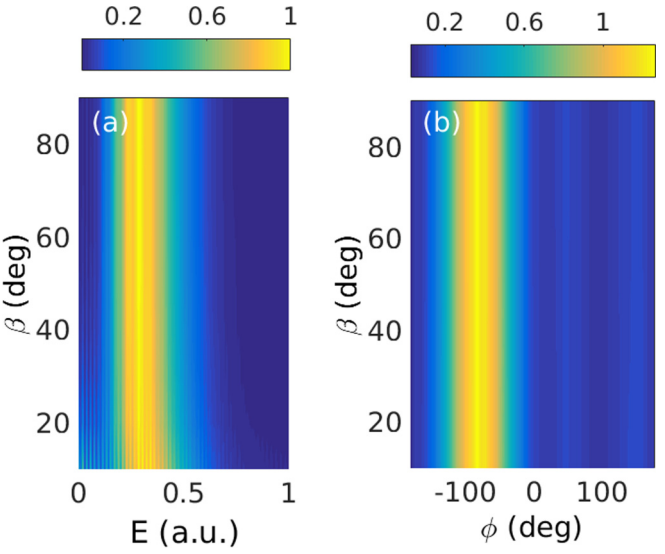

FIG. 4. (a) ATI spectra and (b) angular distributions ($dP/d\phi$) of photoelectrons from Ar($3p_z$) aligned at the angle β relative to the polarization plane of a three-cycle circularly polarized laser pulse with an intensity of 0.1 PW/cm^2 and a wavelength of 800 nm.

ATI spectra obtained at different β values were renormalized to the same peak intensity. The ATI spectra are characterized by a single peak at electron energy of ≈0.32 a.u., corresponding to an electron momentum $k \approx 0.8$ a.u. The peak position in the ATI spectra is independent of the alignment angle β. In Fig. 4(b), we present the angular distribution of photoelectrons in the polarization plane with momentum $k = 0.8 \pm 0.05$ a.u., i.e., $dP/d\phi$, where ϕ is defined relative to the positive k_x axis of the laboratory frame. The PMDs are all rotated counterclockwise; the $dP/d\phi$ distributions peak at $\phi = -82^\circ$ with an offset angle of about 8° compared with the expectation of the simple man's model regardless of the value of β.

It is possible that since we use a short laser pulse, we mainly probe the long-range part of the atomic potential, as was established for atoms in a linearly polarized laser [57,58]. Furthermore, with such a short pulse, the photon energy is not well defined, and multiphoton ionization through low-lying Rydberg states is unlikely. Notice that earlier studies of Ar in linearly polarized laser pulses indicate that multiphoton ionization is enhanced by excitation to low-lying Rydberg states [10,11,59,60]. For these reasons we have also computed PMDs for Ar probed by seven-cycle laser pulses and present ATI spectra for this pulse at various alignment angles β in Fig. 5(a). The ATI spectra are characterized by several multiphoton absorption peaks, with energy difference corresponding to the photon energy (0.057 a.u.) set by the pulse. Also for this pulse, the ATI spectra are invariant to the alignment of the initial orbital. To address the angular part of the PMDs, we focus on a single peak in the ATI spectra, namely, the peak at an energy of 0.32 a.u., corresponding to an electron momentum of 0.8 a.u. In Fig. 5(b) we present angular distributions $dP/d\phi$ for photoelectrons with momentum $k = 0.8 \pm 0.05$ au. We focus on the mean emission peak in the negative k_y plane and hence negative ϕ values. As in the few-cycle limit, the angle ϕ with maximum electron emission is invariant to the alignment of the initial orbital. At the considered pulse duration, the

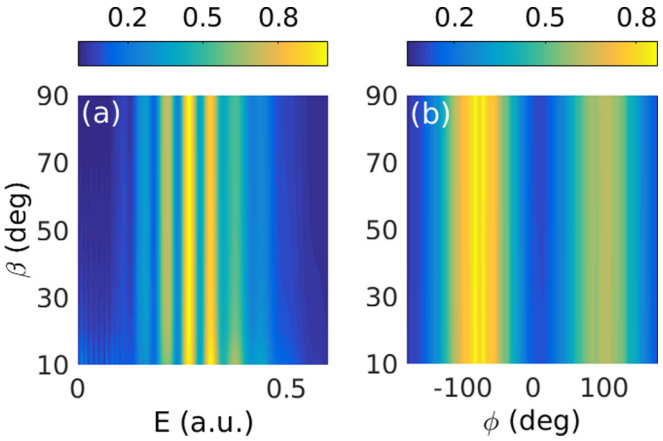

FIG. 5. Same as Fig. 4, but for a seven-cycle laser pulse.

PMD is characterized by a bimodal structure [55], as reflected in Fig. 5(b). The difference in the intensity of the two lines in the figure is a result of the asymmetry still present in the seven-optical-cycle field and the exponential sensitivity of the ionization process to the field strength.

In light of recent research on the imprints of orbital symmetry in PMDs [9,61], we present lateral PMDs for $\mathrm{Ar}(3p_z)$ in Fig. 6. The photoelectron momentum distribution along the laboratory-fixed lateral momentum k_z is calculated for each azimuthal angle ϕ (measured from the positive k_x axis), and the resulting 2D lateral PMDs are presented at alignment angles $\beta = 10°,30°,60°$, and $90°$. At $\beta = 10°$, the signature of the $\mathrm{Ar}(3p_z)$ node is reflected in the lateral PMD as predicted in [9]: the main ionization peak appears off the k_z axis, and the differential ionization probability is significantly more spread along k_z. However, at alignment angles $\beta = 30°,60°$, and $90°$, the lateral PMDs are rather indistinguishable, which shows that the lateral PMD does not always reflect the orbital shape. The lateral momentum

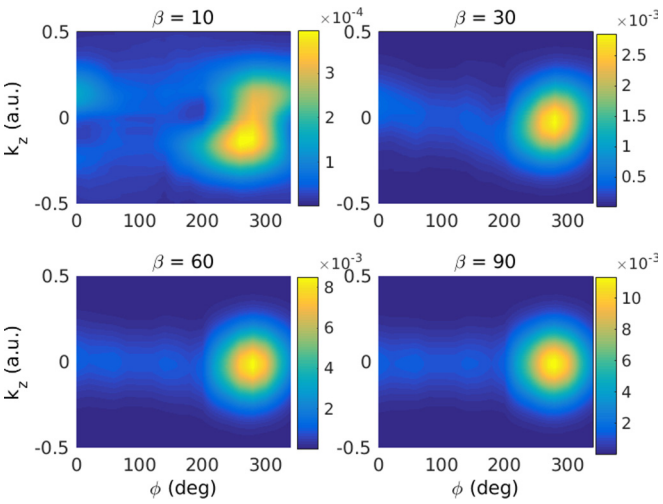

FIG. 6. Lateral PMDs of $\mathrm{Ar}(3p_z)$ at alignment angles $\beta = 10°,30°,60°$, and $90°$, following ionization by a three-cycle, 800-nm, 0.1 PW/cm^2 pulse circularly polarized in the xy plane. The node in the p orbital is only clearly reflected in the lateral PMD when the node is close to the plane of polarization ($\beta = 10°$).

distribution only shows signatures of an angular node of an orbital when its nodal plane is sufficiently close to the plane of polarization. When this is not the case, ionization from the part of the orbital that is in the polarization plane quickly dominates and leads to a lateral distribution similar to that from an s state and suppression of any signature of a nodal structure [30]. From the preceding discussion, we summarize that the lateral PMD shows a signature of the angular node of the rotated $3p_z$ orbital when the node is close to the polarization plane, while the shapes of the ATI spectra, angular distributions, and PMDs in the polarization plane of $\mathrm{Ar}(3p_z)$ are invariant to orbital alignment with respect to the polarization plane of the circularly polarized laser field, regardless of pulse duration. This observation is related to the spherical symmetry of the atomic potential. This symmetry means that the potential is invariant to β rotations and hence that the renormalized PMDs in the polarization plane are insensitive to our choice of β. The results also mean that modeling of strong-field ionization of aligned molecules with just the initial orbital shape and the asymptotic Coulomb potential included would give atomiclike results, i.e., results independent of the underlying higher-order multipoles of the molecular potential. It is therefore of interest to consider the effects of a molecular anisotropic potential on the PMDs, and the study of such effects is the topic of the next section.

B. PMDs from the σ_g state of H_2^+

In this section we explore the effect of molecular alignment on PMDs for the σ_g state of H_2^+ as a prototypical case of a simple molecule with an anisotropic potential. We consider a frozen geometry of H_2^+ with an internuclear separation

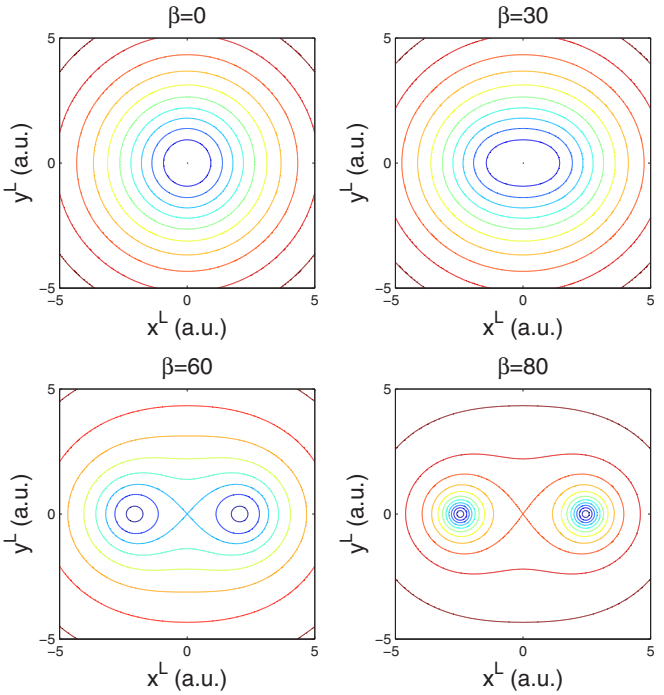

FIG. 7. Cross section of the molecular potential of H_2^+ in the xy plane of the laboratory frame at different alignment angles β (in degrees).

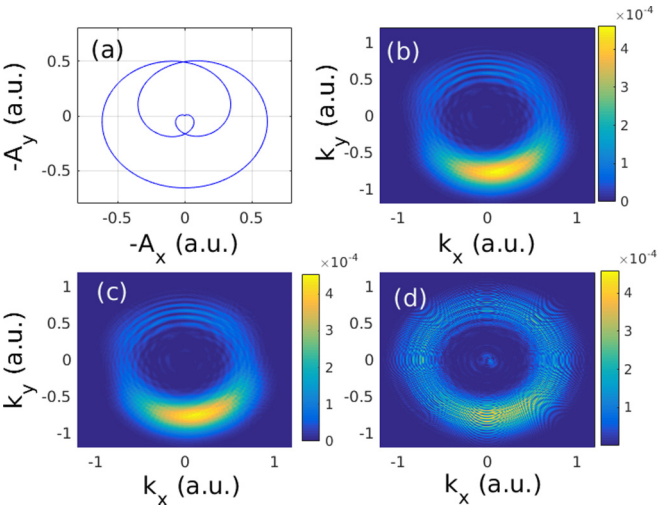

FIG. 8. (a) Parametric plot of $-\vec{A}(t)$ from Eq. (2) and PMDs for Ar $3p_z$ ($\beta = 90°$) obtained by projection on (b) scattering states, (c) asymptotic projection on Coulomb states ($r > 45$ a.u.), and (d) asymptotic projection on plane waves ($r > 45$ a.u.). See the caption of Fig. 3 for laser parameters.

of $R = 5$ a.u. At this distance the ionization energy of the σ_g state is 0.7290 a.u., as obtained by propagation in imaginary time and in good agreement with the table value 0.7244 a.u. [62]. In Fig. 7, we show cross sections of the H_2^+ potential in the xy plane of the laboratory frame at different alignments of the molecular axis relative to that plane. At the alignment angle $\beta = 0°$, the molecular axis (along z^M in Fig. 1) is perpendicular to the plane of laser polarization, and the potential is rotationally invariant in the xy plane of the laboratory frame. At alignment angles different from $\beta = 0°$, the molecular potential is anisotropic in the xy plane of the laboratory frame. The PMDs are expected to reflect this anisotropy of the potential of H_2^+ and its dependence on alignment angle. As β increases, we see a two-center potential building up ($\beta = 60°$ and $\beta = 80°$). In 2D models, the effects on the PMD of electron release at one center and scattering off the neighboring center were previously discussed [33,37].

In calculations of PMDs for H_2^+, due to the nontrivial nature of the H_2^+ scattering states [44–46] and in order to facilitate the calculations of PMDs from the σ_g state, we considered two approaches: projection on Coulomb scattering states vs projection on plane waves, both performed in the asymptotic region of large distance from the electron to the nuclei [53]. These approaches were tested for calculations of PMDs from Ar ($3p_z$) at $\beta = 90$, where exact scattering states are readily available, and the results of these tests are summarized in Fig. 8. The momentum distributions were obtained by projecting on the asymptotic part of the wave packet, that is, at $r > 45$ a.u., and the projections were performed at the end of the laser pulse, without further field-free propagation. Clearly, whereas the plane wave approach is unsatisfactory, projecting on Coulomb waves gives excellent agreement with the PMDs obtained by projection on the scattering states of Ar. Hence PMDs for ionization from the σ_g state of H_2^+ were calculated by asymptotic projection on Coulomb waves. The results of this methodology were checked for convergence with respect to integration volume and field-free postpulse propagation.

PMDs corresponding to the σ_g state of H_2^+ are presented in Fig. 9 as obtained at different alignments of the molecular axis relative to the xy plane of the laboratory frame. The results show a strong dependence of PMDs on the alignment angle. At alignment angle $\beta = 0°$, the molecular axis is perpendicular to the plane of circular laser polarization, and the resulting PMD resembles those for atomic targets (see PMDs for the $3p$ orbital in Ar in Fig. 3). The similarity of the atomic and molecular cases for this geometry may be understood by noting the rotational symmetry of the molecular potential.

At alignment angles $\beta = 10°$ and $20°$, the obtained PMDs are rotated clockwise compared to that obtained at $\beta = 0°$; the offset angle is minimal at $\beta = 20°$. This behavior of the PMDs with changing alignment angle may be attributed to a change of the molecular potential in the polarization plane, as can be seen in Fig 7. A comparison of the $\beta = 0°, 10°$, and $20°$ results in Fig. 9 is also interesting in relation to attoclock experiments [15,16,35] since the results show that the shift in the peak of the PMD is very sensitive to terms in the molecular potential beyond the Coulombic monopole.

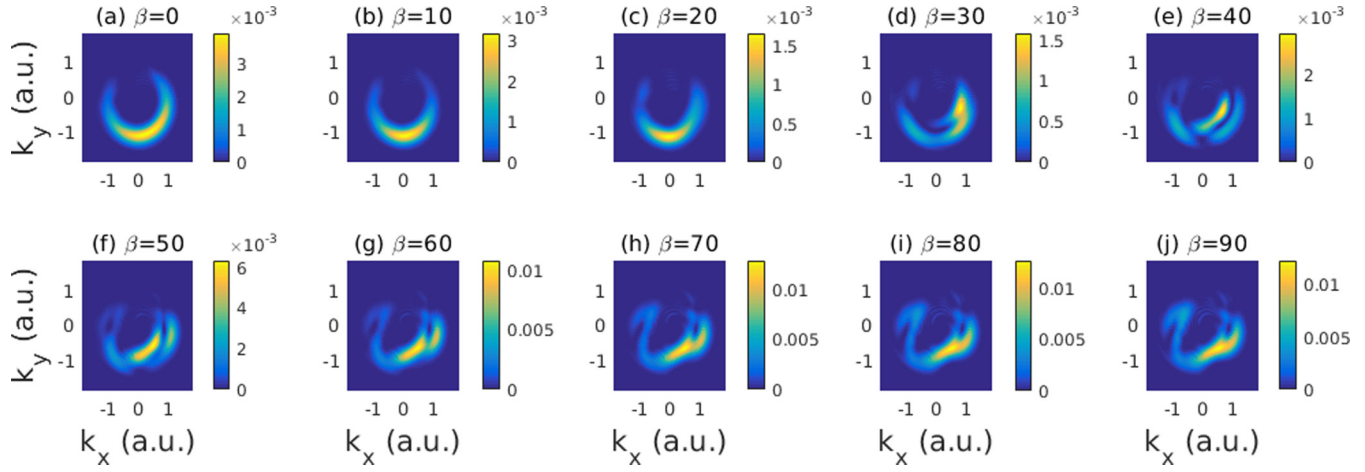

FIG. 9. PMDs in the xy plane from the σ_g state of H_2^+ at $R = 5$ a.u. probed at different alignment angles β (in degrees). The parameters of the circularly polarized laser are as follows: intensity of 0.2 PW/cm^2, two cycles, and wavelength of 800 nm.

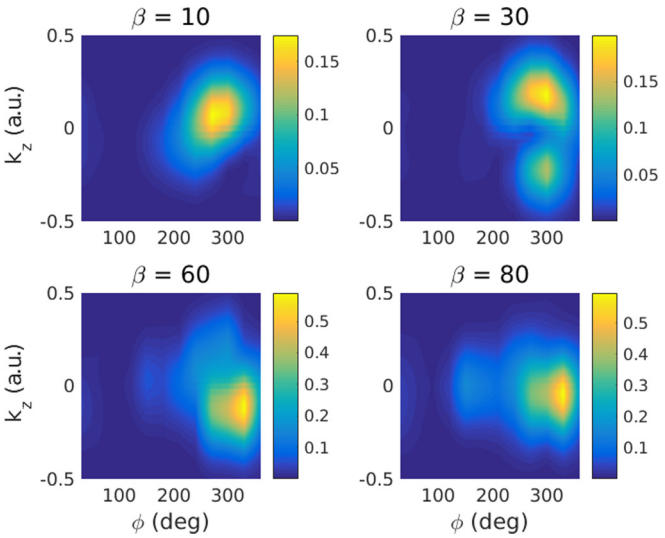

FIG. 10. Lateral PMDs from $H_2{}^+(\sigma_g)$ ($R = 5$ a.u.) probed by a laser pulse at alignment angles $\beta = 10°,30°,60°$, and $80°$. The parameters of the circularly polarized laser are as follows: intensity of 0.2 PW/cm^2, two cycles, and wavelength of 800 nm.

At $\beta = 30°$, new features emerge in the PMDs. These change between $\beta = 30°$ and $\beta = 70°$ and remain largely unchanged for alignment angles $\beta = 70°,80°$, and $90°$. In Ref. [33], where the PMDs for $H_2{}^+$ were obtained from 2D calculations and for the molecular axis confined to the polarization plane, it was suggested that the PMDs have two components emerging respectively from direct electrons and electrons scattering off the neighboring nucleus and that the scattered components show larger offset angles and reach higher momenta than the direct electrons. In the 3D case for the present set of parameters with the molecular axis close to or in the polarization plane ($\beta = 80°$ and $\beta = 90°$) we do not observe any momenta larger than those present for the other alignments, and moreover the offset angle for the peak in the PMD is similar to the result for the other alignments.

In Fig. 10 we present lateral PMDs for $H_2{}^+$ at alignment angles $\beta = 10°,30°,60°$, and $80°$. The lateral PMDs show a strong dependence on the alignment angle β. Since the initial orbital is σ_g, this modulation does not come from the initial orbital, but rather from the anisotropic potential and the excitation and ionization dynamics. At $\beta = 0°$ (not shown) the molecular wave function preserves its symmetry during the field: the initial state is even with respect to reflection in the laboratory xy plane, and the field is in that plane, so the PMD is atomic s-like for the initial σ_g state. At $\beta = 10$ there is a shift of the peak of the distribution towards positive k_z values. At $\beta = 30°$, there is a modulation with two local maxima, one at positive k_z and a smaller one at negative k_z. At $\beta = 60°$ the peak of the distribution has shifted towards negative k_z, and finally, at $\beta = 80°$ the distribution peaks at $k_z \simeq 0$. We may understand these findings from the anisotropy of the molecular potential, the asymmetry in the initial ionization step in the few-cycle pulse, and the excitation to the σ_u state, which has a node. For example, at $\beta = 10°$ there is no strong coupling to the σ_u state (this is a parallel transition), so there is no signature of a node in the lateral PMD. There is, however, an asymmetry in the ionization step induced by the short pulse and the fixed carrier envelope phase (CEP), and this means that mainly one end of the molecular potential is felt by the outgoing electron, leading overall to the shift up in the distribution. As another example, consider $\beta = 30°$. In this case, we have checked that a change in the CEP by π radians shifts the distribution by $180°$ in ϕ and leads to a reflection of the distribution with respect to $k_z = 0$, in accordance with the change in the effective molecular potential seen by the outgoing electron upon that CEP change. Simultaneously, at $\beta = 30°$ there is a relatively stronger coupling to the σ_u state, and the resulting double-peak structure in the lateral PMD is consistent with ionization out of this state.

IV. CONCLUSIONS AND OUTLOOK

We calculated PMDs for aligned $3p$ orbitals of Ar and for $H_2{}^+(\sigma_g)$ probed by few-cycle, circularly polarized laser pulses with a laser intensity of 0.1 PW/cm^2 for Ar [0.2 PW/cm^2 for $H_2{}^+(\sigma_g)$] at a wavelength of 800 nm. In the atomic case, the calculated renormalized PMDs in the polarization plane and the offset angle do not depend on the alignment angle of the atomic orbital. Moreover, the lateral momentum distribution does not always convey information about orbital alignment. Turning to the molecular case study of $H_2{}^+(\sigma_g)$, the calculated PMDs in the polarization plane and lateral PMDs vary with the alignment of the molecular axis relative to the plane of laser polarization. The reason for this is the asymmetry of the molecular potential due to the presence of two nuclei. The present results show that theoretical models aiming at exploring the PMDs, for example, through an analysis of angular shifts as in the attoclock scheme, generally have to include not only information about the orbital and the Coulomb potential but also some excited-state information as well as the specifics of the higher-order multipoles of the short-ranged part of the molecular potential.

ACKNOWLEDGMENTS

This work was supported by the ERC-StG (Project No. 277767-TDMET), the VKR center of excellence, QUSCOPE, and the Aarhus University Research Foundation (AUFF). The computations were performed on the cluster of the Centre of Scientific Computing Aarhus (CSCAA).

[1] G. G. Paulus, F. Grasbon, H. Walther, P. Villoresi, M. Nisoli, S. Stagira, E. Priori, and S. De Silvestri, Absolute-phase phenomena in photoionization with few-cycle laser pulses, Nature (London) **414**, 182 (2001).

[2] D. B. Milošević, G. G. Paulus, and W. Becker, Phase-Dependent Effects of a Few-Cycle Laser Pulse, Phys. Rev. Lett. **89**, 153001 (2002).

[3] Yuan Minghu, Wang Dandan, Chen Junsheng, Fu Aiping, Tian Fenghui, and Chu Tianshu, Influence of pulse duration

on above-threshold ionization in intensive circularly polarized laser field, Can. J. Phys. **93**, 93 (2015).

[4] C. P. J. Martiny and L. B. Madsen, Symmetry of Carrier-Envelope Phase Difference Effects in Strong-Field, Few-Cycle Ionization of Atoms and Molecules, Phys. Rev. Lett. **97**, 093001 (2006).

[5] C. P. J. Martiny and L. B. Madsen, Finite-bandwidth effects in strong-field ionization of atoms by few-cycle circularly polarized laser pulses, Phys. Rev. A **76**, 043416 (2007).

[6] C. P. J. Martiny and L. B. Madsen, Ellipticity dependence of the validity of the saddle-point method in strong-field ionization by few-cycle laser pulses, Phys. Rev. A **78**, 043404 (2008).

[7] G. L. Kamta and A. D. Bandrauk, Phase Dependence of Enhanced Ionization in Asymmetric Molecules, Phys. Rev. Lett. **94**, 203003 (2005).

[8] C. P. J. Martiny, M. Abu-samha, and L. B. Madsen, Ionization of oriented targets by intense circularly polarized laser pulses: Imprints of orbital angular nodes in the two-dimensional momentum distribution, Phys. Rev. A **81**, 063418 (2010).

[9] I. Petersen, J. Henkel, and M. Lein, Signatures of Molecular Orbital Structure in Lateral Electron Momentum Distributions From Strong-Field Ionization, Phys. Rev. Lett. **114**, 103004 (2015).

[10] A. S. Alnaser, C. M. Maharjan, P. Wang, and I. V. Litvinyuk, Multi-photon resonant effects in strong-field ionization: Origin of the dip in experimental longitudinal momentum distributions, J. Phys. B **39**, L323 (2006).

[11] M. Abu-samha and L. B. Madsen, From multiphoton to tunnelling ionization of neon and argon, J. Phys. B **41**, 151001 (2008).

[12] F. Krausz and M. Ivanov, Attosecond physics, Rev. Mod. Phys. **81**, 163 (2009).

[13] C. Lux, M. Wollenhaupt, T. Bolze, Q. Liang, J. Köhler, C. Sarpe, and T. Baumert, Circular dichroism in the photoelectron angular distributions of camphor and fenchone from multiphoton ionization with femtosecond laser pulses, Angew. Chem., Int. Ed. **51**, 5001 (2012).

[14] C. Lux, M. Wollenhaupt, C. Sarpe, and T. Baumert, Photoelectron circular dichroism of bicyclic ketones from multiphoton ionization with femtosecond laser pulses, ChemPhysChem **16**, 115 (2015).

[15] L. Torlina, F. Morales, J. Kaushal, I. Ivanov, A. Kheifets, A. Zielinski, A. Scrinzi, H. G. Muller, S. Sukiasyan, M. Ivanov, and O. Smirnova, Interpreting attoclock measurements of tunnelling times, Nat. Phys. **11**, 503 (2015).

[16] P. Eckle, A. N. Pfeiffer, C. Cirelli, A. Staudte, R. Dörner, H. G. Muller, M. Buttiker, and U. Keller, Attosecond ionization and tunneling delay time measurements in helium, Science **322**, 1525 (2008).

[17] L. J. Zipp, A. Natan, and P. H. Bucksbaum, Probing electron delays in above-threshold ionization, Optica **1**, 361 (2014).

[18] A. N. Pfeiffer, C. Cirelli, M. Smolarski, R. Dörner, and U. Keller, Timing the release in sequential double ionization, Nat. Phys. **7**, 428 (2011).

[19] A. N. Pfeiffer, C. Cirelli, M. Smolarski, D. Dimitrovski, M. Abu-samha, L. B. Madsen, and U. Keller, Attoclock reveals natural coordinates of the laser-induced tunnelling current flow in atoms, Nat. Phys. **8**, 76 (2012).

[20] L. Torlina, J. Kaushal, and O. Smirnova, Time-resolving electron-core dynamics during strong-field ionization in circularly polarized fields, Phys. Rev. A **88**, 053403 (2013).

[21] X. Xie, Two-Dimensional Attosecond Electron Wave-Packet Interferometry, Phys. Rev. Lett. **114**, 173003 (2015).

[22] T. Zimmermann, S. Mishra, B. R. Doran, D. F. Gordon, and A. S. Landsman, Tunneling Time and Weak Measurement in Strong Field Ionization, Phys. Rev. Lett. **116**, 233603 (2016).

[23] F. Mauger, C. Chandre, and T. Uzer, Recollisions and Correlated Double Ionization With Circularly Polarized Light, Phys. Rev. Lett. **105**, 083002 (2010).

[24] M. Murakami and Shih-I Chu, Photoelectron momentum distributions of the hydrogen atom driven by multicycle elliptically polarized laser pulses, Phys. Rev. A **93**, 023425 (2016).

[25] J. Maurer, D. Dimitrovski, L. Christensen, L. B. Madsen, and H. Stapelfeldt, Molecular-Frame 3D Photoelectron Momentum Distributions by Tomographic Reconstruction, Phys. Rev. Lett. **109**, 123001 (2012).

[26] A. Staudte, S. Patchkovskii, D. Pavičić, H. Akagi, O. Smirnova, D. Zeidler, M. Meckel, D. M. Villeneuve, R. Dörner, M. Yu. Ivanov, and P. B. Corkum, Angular Tunneling Ionization Probability of Fixed-in-Space H_2 Molecules in Intense Laser Pulses, Phys. Rev. Lett. **102**, 033004 (2009).

[27] H. Akagi, T. Otobe, A. Staudte, A. Shiner, F. Turner, R. Dorner, D. M. Villeneuve, and P. B. Corkum, Laser tunnel ionization from multiple orbitals in HCl, Science **325**, 1364 (2009).

[28] L. Holmegaard, J. L. Hansen, L. Kalhoj, S. Louise Kragh, H. Stapelfeldt, F. Filsinger, J. Kupper, G. Meijer, D. Dimitrovski, M. Abu-samha, C. P. J. Martiny, and L. B. Madsen, Photoelectron angular distributions from strong-field ionization of oriented molecules, Nat. Phys. **6**, 428 (2010).

[29] D. Dimitrovski, J. Maurer, H. Stapelfeldt, and L. B. Madsen, Low-Energy Photoelectrons in Strong-Field Ionization By Laser Pulses With Large Ellipticity, Phys. Rev. Lett. **113**, 103005 (2014).

[30] D. Dimitrovski, J. Maurer, H. Stapelfeldt, and L. B. Madsen, Strong-field ionization of three-dimensionally aligned naphthalene molecules: Orbital modification and imprints of orbital nodal planes, J. Phys. B **48**, 245601 (2015).

[31] D. Dimitrovski, J. Maurer, H. Stapelfeldt, and L. B. Madsen, Observation of low-energy electrons in the photoelectron energy distribution from strong-field ionization of naphthalene by circularly polarized pulses, J. Phys. B **48**, 121001 (2015).

[32] D. Dimitrovski and L. B. Madsen, Theory of low-energy photoelectrons in strong-field ionization by laser pulses with large ellipticity, Phys. Rev. A **91**, 033409 (2015).

[33] P.-L. He, N. Takemoto, and F. He, Photoelectron momentum distributions of atomic and molecular systems in strong circularly or elliptically polarized laser fields, Phys. Rev. A **91**, 063413 (2015).

[34] M. Ohmi, O. I. Tolstikhin, and T. Morishita, Analysis of a shift of the maximum of photoelectron momentum distributions generated by intense circularly polarized pulses, Phys. Rev. A **92**, 043402 (2015).

[35] A. S. Landsman, M. Weger, J. Maurer, R. Boge, A. Ludwig, S. Heuser, C. Cirelli, L. Gallmann, and U. Keller, Ultrafast resolution of tunneling delay time, Optica **1**, 343 (2014).

[36] C. P. J. Martiny, M. Abu-samha, and L. B. Madsen, Counterintuitive angular shifts in the photoelectron momentum distribution for atoms in strong few-cycle circularly polarized laser pulses, J. Phys. B **42**, 161001 (2009).

[37] W. Yang, Z. Sheng, X. Feng, M. Wu, Z. Chen, and X. Song, Molecular photoelectron holography with circularly polarized laser pulses, Opt. Express **22**, 2519 (2014).

[38] Z. C. Li and F. He, *Ab initio* non-Born-Oppenheimer simulations of rescattering dissociation of H_2 in strong infrared laser fields, Phys. Rev. A **90**, 053423 (2014).

[39] N. V. Golubev and A. I. Kuleff, Control of charge migration in molecules by ultrashort laser pulses, Phys. Rev. A **91**, 051401 (2015).

[40] M. Spanner, S. Gräfe, S. Chelkowski, D. Pavicic, M. Meckel, D. Zeidler, A. B. Bardon, B. Ulrich, A. D. Bandrauk, D. M. Villeneuve, R. Dörner, P. B. Corkum, and A. Staudte, Coulomb asymmetry and sub-cycle electron dynamics in multiphoton multiple ionization of H_2, J. Phys. B **45**, 194011 (2012).

[41] L. Yue and L. B. Madsen, Inter- and intracycle interference effects in strong-field dissociative ionization, Phys. Rev. A **93**, 031401 (2016).

[42] M. Odenweller, J. Lower, K. Pahl, M. Schütt, J. Wu, K. Cole, A. Vredenborg, L. Ph. Schmidt, N. Neumann, J. Titze, T. Jahnke, M. Meckel, M. Kunitski, T. Havermeier, S. Voss, M. Schöffler, H. Sann, J. Voigtsberger, H. Schmidt-Böcking, and R. Dörner, Electron emission from H_2^+ in strong laser fields, Phys. Rev. A **89**, 013424 (2014).

[43] M. Odenweller, N. Takemoto, A. Vredenborg, K. Cole, K. Pahl, J. Titze, L. Ph. H. Schmidt, T. Jahnke, R. Dörner, and A. Becker, Strong Field Electron Emission from Fixed in Space H_2^+ ions, Phys. Rev. Lett. **107**, 143004 (2011).

[44] J. Fernández and L. B. Madsen, Energy-resolved photoelectron angular distributions of H_2^+ in intense femtosecond laser pulses, J. Phys. B **42**, 021001 (2009).

[45] J. Fernández and L. B. Madsen, Alignment dependence in above-threshold ionization of H_2^+: Role of intermediate resonances, J. Phys. B **42**, 085602 (2009).

[46] J. Fernández and L. B. Madsen, Above-threshold ionization, energy-resolved photoelectron angular distributions, and momentum distributions of H_2^+ in intense femtosecond laser pulses, Phys. Rev. A **79**, 063406 (2009).

[47] T. K. Kjeldsen, L. A. A. Nikolopoulos, and L. B. Madsen, Solving the m-mixing problem for the three-dimensional time-dependent Schrödinger equation by rotations: Application to strong-field ionization of H_2^+, Phys. Rev. A **75**, 063427 (2007).

[48] H. G. Muller, An efficient propagation scheme for the time-dependent Schrödinger equation in the velocity gauge, Laser Phys. **9**, 138 (1999).

[49] J. M. Ngoko Djiokap, N. L. Manakov, A. V. Meremianin, S. X. Hu, L. B. Madsen, and A. F. Starace, Nonlinear Dichroism in Back-To-Back Double Ionization of He by an Intense Elliptically Polarized Few-Cycle Extreme Ultraviolet Pulse, Phys. Rev. Lett. **113**, 223002 (2014).

[50] J. M. Ngoko Djiokap, S. X. Hu, L. B. Madsen, N. L. Manakov, A. V. Meremianin, and A. F. Starace, Electron Vortices in Photoionization by Circularly Polarized Attosecond Pulses, Phys. Rev. Lett. **115**, 113004 (2015).

[51] J. M. Ngoko Djiokap, A. V. Meremianin, N. L. Manakov, S. X. Hu, L. B. Madsen, and A. F. Starace, Multistart spiral electron vortices in ionization by circularly polarized UV pulses, Phys. Rev. A **94**, 013408 (2016).

[52] H. G. Muller and F. C. Kooiman, Bunching and Focusing of Tunneling Wave Packets in Enhancement of High-Order Above-Threshold Ionization, Phys. Rev. Lett. **81**, 1207 (1998).

[53] L. B. Madsen, L. A. A. Nikolopoulos, T. K. Kjeldsen, and J. Fernandez, Extracting continuum information from $\Psi(t)$ in time-dependent wave-packet calculations, Phys. Rev. A **76**, 063407 (2007).

[54] L. Argenti, R. Pazourek, J. Feist, S. Nagele, M. Liertzer, E. Persson, J. Burgdörfer, and E. Lindroth, Photoionization of helium by attosecond pulses: Extraction of spectra from correlated wave functions, Phys. Rev. A **87**, 053405 (2013).

[55] N. I. Shvetsov-Shilovski, D. Dimitrovski, and L. B. Madsen, Ionization in elliptically polarized pulses: Multielectron polarization effects and asymmetry of photoelectron momentum distributions, Phys. Rev. A **85**, 023428 (2012).

[56] N. I. Shvetsov-Shilovski, D. Dimitrovski, and L. B. Madsen, Ehrenfest's theorem and the validity of the two-step model for strong-field ionization, Phys. Rev. A **87**, 013427 (2013).

[57] M. Abu-samha, D. Dimitrovski, and L. B. Madsen, The role of the atomic potential in the regime of strong-field tunneling ionization: Imprints on longitudinal and 2D momentum distributions, J. Phys. B **41**, 245601 (2008).

[58] K. I. Dimitriou, D. G. Arbó, S. Yoshida, E. Persson, and J. Burgdörfer, Origin of the double-peak structure in the momentum distribution of ionization of hydrogen atoms driven by strong laser fields, Phys. Rev. A **70**, 061401 (2004).

[59] C. M. Maharjan, A. S. Alnaser, I. Litvinyuk, P. Ranitovic, and C. L. Cocke, Wavelength dependence of momentum-space images of low-energy electrons generated by short intense laser pulses at high intensities, J. Phys. B **39**, 1955 (2006).

[60] A. Rudenko, K. Zrost, C. D. Schröter, V. L. B. de Jesus, B. Feuerstein, R. Moshammer, and J. Ullrich, Resonant structures in the low-energy electron continuum for single ionization of atoms in the tunneling regime, J. Phys. B **37**, L407 (2004).

[61] M. Abu-samha and L. B. Madsen, Interrogation of orbital structure by elliptically polarized intense femtosecond laser pulses, Phys. Rev. A **84**, 023411 (2011).

[62] T. E. Sharp, Potential-energy curves for molecular hydrogen and its ions, At. Data Nucl. Data Tables **2**, 119 (1970).